Linearized Frequency-Domain Gust Analysis and Adjoint-Based Sensitivities

Kevin E. Jacobson,* Andrew S. Thelen,† Bret K. Stanford‡
NASA Langley Research Center, Hampton, VA, 23681

Gust analysis is added to a linearized frequency-domain method in FUN3D, a NASA computational fluid dynamics solver. The method linearizes about a nonlinear static equilibrium condition and is therefore appropriate for problems with small perturbations such as transonic stochastic gust analysis. In addition to the gust analysis, adjoint-based sensitivities of stochastic gust constraints are implemented for multidisciplinary design optimization. The linearized frequency-domain gust model and adjoint-based sensitivities are described and verified. The method is applied to an optimization for mass minimization of the AGARD 445.6 wing subject to a stochastic gust constraint limiting the displacement of the wing tip.

I. Introduction

Aeroelastic gust response and ride quality are important design considerations for aircraft, particularly as the industry shifts toward more flexible, higher aspect ratio wings for efficiency. Many aircraft fly in the transonic regime, and the conditions may necessitate the use of nonlinear aerodynamic modeling such as Computational Fluid Dynamics (CFD). The high cost of unsteady CFD creates a challenge that must be overcome to make CFD-based gust modeling tractable for design optimization. If this barrier can be overcome, simultaneous design of the vehicle and aeroservoelastic control laws should lead to a more efficient overall design. There are examples in the literature of CFD-based aeroservoelastic control law designs for gust load alleviation (GLA) [1]. Typically, the CFD-based aerodynamics are processed into a form suitable for control law design such as a reduced order model [2]. However, to the authors' knowledge, simultaneous design of the vehicle and control laws for GLA has been limited to linear aerodynamics [3, 4]. In order to introduce CFD into this type of problem, tractable gust modeling must be developed including adjoint-based sensitivities to reduce the cost of design optimization.

Time-domain CFD is very general and can be applied to gust constraints on relatively small design cases [5], but it is currently too expensive for application to more complete aircraft optimization problems. Nonlinear frequency-domain approaches such as harmonic balance and time spectral methods can be faster when a periodic assumption is valid [6–8]. When there are small perturbations, Linearized Frequency-Domain (LFD) methods are even more efficient than nonlinear frequency domain methods [9, 10]. In Jacobson et al. [11], LFD for flutter analysis was added to the FUN3D Stabilized Finite-Element flow solver (FUN3D/SFE). Adjoint-based sensitivities were then added [12] and utilized for flutter-constrained design optimization [13]. In this work, the LFD solver in FUN3D/SFE is extended to allow gust perturbations. The corresponding adjoint-based sensitivities are added and demonstrated on a simple optimization problem, mass minimization of the AGARD 445.6 wing [14] subject to gust-based constraint. This work represents a step toward CFD-based stochastic gust constraints, ride quality constraints, and GLA control law design in multidisciplinary optimization.

II. Methodology

FUN3D is an unstructured CFD code developed at the NASA Langley Research Center [15–18]. The FUN3D/SFE discretization is a Streamline-Upwind Petrov-Galerkin (SUPG) finite-element solver [19, 20]. The governing equations in FUN3D/SFE include the RANS equations with the negative Spalart-Allmaras turbulence model [21]; however, the simulations in this work are all inviscid. To account for mesh movement, these equations are solved using an Arbitrary Lagrangian-Eulerian (ALE) formulation [20]:

$$\int_{\Omega(t)} (N+P)\left[\dot{\mathbf{q}} + \nabla\cdot(\mathbf{F} - \mathbf{q}\,\dot{\mathbf{x}}_G) + \mathbf{q}\nabla\cdot\dot{\mathbf{x}}_G - \mathbf{S}\right] d\Omega = 0, \tag{1}$$

*Research Aerospace Engineer, Aeroelasticity Branch, kevin.e.jacobson@nasa.gov, AIAA Member.
†Research Aerospace Engineer, Aeroelasticity Branch, AIAA Member.
‡Research Aerospace Engineer, Aeroelasticity Branch, AIAA Associate Fellow.

where N is the Galerkin weighting function, P is the Petrov-Galerkin weighting function described in Ref. [19], $\mathbf{q}$ is the flow state vector, $\mathbf{x}_G$ is the vector of volume mesh coordinates, $\mathbf{F}$ is the flux vector, $\mathbf{S}$ is the source term, and Newton notation for time derivatives is used. FUN3D applies a linear elasticity analogy to deform the mesh during aeroelastic simulations.

A. Gust Modeling

This work adds the Field Velocity Method (FVM) for gust modeling [22] to FUN3D/SFE. For FVM, the gust velocity in the domain is applied using the grid velocity without actually displacing the grid points:

$$\dot{\mathbf{x}}_{G,total} = \dot{\mathbf{x}}_G - \mathbf{u}_G, \tag{2}$$

where $\dot{\mathbf{x}}_G$ is the true grid velocity based on the mesh motion, and $\mathbf{u}_G$ is the prescribed gust velocity. FVM is an approximation that does not account for the feedback of the computed flow on the prescribed gust itself. The Split Velocity Method (SVM) is derived with no simplifications from the ALE form of the governing equations and results in an additional source term that accounts for this effect; however, as demonstrated in Boulbrachene et al. [23], the differences in the two versions of gust modeling are negligible for vertical gusts. Since the gusts modeled in this work are vertical gusts, the simpler FVM approach is used.

The first verification of the FVM implementation is a steady, uniform gust in the vertical direction. For steady uniform gusts, the source term from SVM is zero; and therefore, a change in angle of attack of a steady simulation is equivalent to a uniform vertical gust with FVM and a reduction in the freestream speed to maintain the same total velocity magnitude ($M^2_{\infty,gust} + w^2_{gust} = M^2_{\infty,0}$ where w_{gust} is nondimensionalized by the speed of sound and $M_{\infty,0}$ is the freestream Mach number of the steady simulation). Table 1 compares the forces for an inviscid NACA 64A010 airfoil at Mach 0.4 and 0° angle of attack subjected to a 1° increase angle of attack. The first row corresponds to changing the angle of attack at the farfield boundary conditions, and the second row is the gust-based equivalent. The x and z components of the forces agree to 12 and 11 significant figures, respectively.

The FVM has previously been implemented and verified in the node-centered finite volume solver in FUN3D (FUN3D/FV) [24]. Figure 1 compares the two discretizations for a time-domain gust problem. From an initial steady state, the inviscid NACA 64A010 at Mach 0.4 is subjected to a sinusoidal gust. The vertical gust has a magnitude of Mach 0.025 and reduced frequency of 0.5. There are small differences in the amplitude of the lift coefficient due to differences in accuracy of the discretizations on the same mesh, but overall there is good agreement between the two discretizations, which indicates that the FVM gust model has been implemented properly in FUN3D/SFE.

B. Linearized Frequency-Domain Analysis

The linearized stochastic gust analysis requires two types of perturbations to the LFD version of the aerodynamic governing equations: perturbations in the form of structural mode motion and gust velocity. To derive both forms, the SUPG equations for the flow, Eq. 1, are rewritten as:

$$\mathbf{A}(\mathbf{q}, \dot{\mathbf{q}}, \mathbf{x}_G, \dot{\mathbf{x}}_G, \mathbf{u}_G) := \mathbf{M}_A(\mathbf{q}, \mathbf{x}_G, \dot{\mathbf{x}}_G, \mathbf{u}_G)\ \dot{\mathbf{q}} + \mathbf{R}(\mathbf{q}, \mathbf{x}_G, \dot{\mathbf{x}}_G, \mathbf{u}_G) = 0, \tag{3}$$

where $\mathbf{M}_A$ is the mass matrix, which is a function of the state due to use of the Petrov-Galerkin weighting function, and $\mathbf{R}$ is the spatial residual. The steady flow residual is a simplification with the time derivatives set to zero:

$$\mathbf{A}_0\,(\mathbf{q}_0, \mathbf{x}_{G0}) := \mathbf{R}(\mathbf{q}_0, \mathbf{x}_{G0}) = 0. \tag{4}$$

Table 1 Verification of FVM gust implementation with a steady uniform gust in the vertical direction compared to an angle of attack change. Coefficient of force in the x and z directions.

Method	C_x	C_z
Angle of Attack	−**1.568666493700**e-03	**1.270856113**900e-01
Vertical Gust	−**1.568666493704**e-03	**1.270856113**859e-01

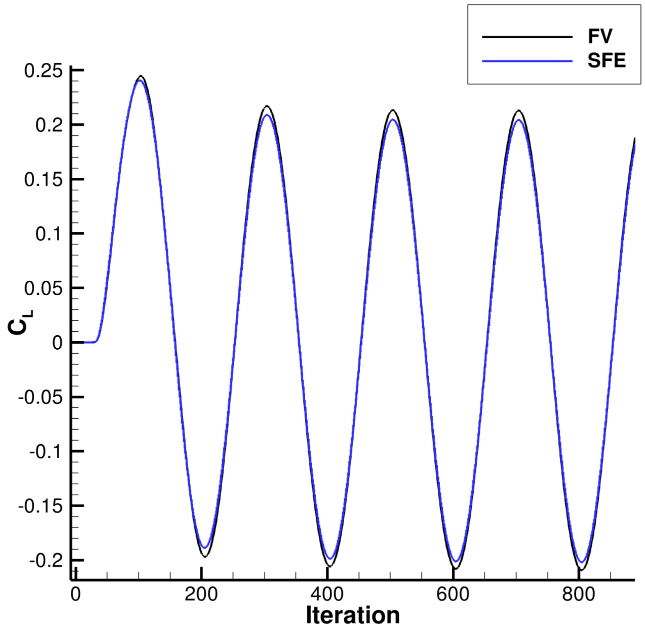

Fig. 1 Time histories of lift for FUN3D/FV and FUN3D/SFE of an NACA 64A010 airfoil subject to a sinusoidal gust.

1. Linearized Frequency Domain - Structural Mode Perturbation

The time-dependent mesh and solution vectors in Eq. 3 are assumed to be the superposition of an equilibrium state and small, harmonic perturbations due to motion of structural modes, n, at frequency ω_k:

$$\mathbf{x}_G(t) := \mathbf{x}_{G0} + \sum_{k}^{n_k} \sum_{n}^{n_n} \alpha_{k,n} \hat{\mathbf{x}}_{G,n} e^{i\omega_k t}, \tag{5}$$

$$\mathbf{q}(t) := \mathbf{q}_0 + \sum_{k}^{n_k} \sum_{n}^{n_n} \alpha_{k,n} \hat{\mathbf{q}}_{n,k} e^{i\omega_k t}, \tag{6}$$

where $\hat{\mathbf{x}}_{G,n}$ is a spatially varying displacement field corresponding to a unit displacement of the structural mode n, $\alpha_{k,n}$ is an amplitude of mode n at frequency ω_k, and $\hat{\mathbf{q}}_{n,k}$ is the Fourier coefficient for the flow response to motion of mode n at frequency ω_k with a unit amplitude. The governing equations of the flow are linearized about the equilibrium solution and simplified to:

$$\mathbf{A}_{LFD,n,k}\left(\mathbf{x}_{G0}, \mathbf{q}_0, \hat{\mathbf{x}}_{G,n}, \hat{\mathbf{q}}_{n,k}\right) := \left(i\omega_k \left.\mathbf{M}_A\right|_{\mathbf{x}_{G0},\mathbf{q}_0} + \left.\frac{\partial \mathbf{R}}{\partial \mathbf{q}}\right|_{\mathbf{x}_{G0},\mathbf{q}_0}\right)\hat{\mathbf{q}}_{n,k} + \left.\frac{\partial \mathbf{R}}{\partial \mathbf{x}_G}\right|_{\mathbf{x}_{G0},\mathbf{q}_0} \hat{\mathbf{x}}_{G,n} + i\omega_k \left.\frac{\partial \mathbf{R}}{\partial \dot{\mathbf{x}}_G}\right|_{\mathbf{x}_{G0},\mathbf{q}_0} \hat{\mathbf{x}}_{G,n} = 0. \tag{7}$$

This linear system is solved once for each combination of frequency of interest (ω_k) and mesh motion input ($\hat{\mathbf{x}}_{G,n}$), which is computed by propagating the mode shapes of the structure through the CFD volume mesh deformation process. Equation 7 is solved with a generalized minimum residual method (GMRES) [25] implemented in the Sparse Linear Algebra Toolkit (SLAT) [26]. From $\hat{\mathbf{q}}_{n,k}$ and $\hat{\mathbf{x}}_{G,n}$, Fourier coefficients of surface force perturbations are computed as:

$$\hat{\mathbf{f}}_{n,k} := \left.\frac{\partial \mathbf{f}}{\partial \mathbf{q}}\right|_{\mathbf{x}_{G0},\mathbf{q}_0} \hat{\mathbf{q}}_{n,k} + \left.\frac{\partial \mathbf{f}}{\partial \mathbf{x}_G}\right|_{\mathbf{x}_{G0},\mathbf{q}_0} \hat{\mathbf{x}}_{G,n} + i\omega_k \left.\frac{\partial \mathbf{f}}{\partial \dot{\mathbf{x}}_G}\right|_{\mathbf{x}_{G0},\mathbf{q}_0} \hat{\mathbf{x}}_{G,n}, \tag{8}$$

where $\mathbf{f}$ is the function to calculate the aerodynamic force distribution. Generalized aerodynamic forces (GAFs) can be calculated by taking the inner product of the linearized force perturbations and the mode shapes projected onto the aerodynamic surface:

$$\bar{\mathbf{Q}}_{ss}\left(i\omega_k\right)_{m,n} := \mathbf{\Phi}_{A,m}^T \hat{\mathbf{f}}_{n,k}, \tag{9}$$

where $\mathbf{\Phi}_{A,m}$ is the mode shape for mode m projected onto the aerodynamic surface. At a given frequency, the entries of the matrix of GAFs, $\bar{\mathbf{Q}}_{ss}\left(i\omega_k\right)$, represents the modal force on mode m due to harmonic motion of mode n. This collection of GAFs will be referenced as the structure-on-structure GAFs. For flutter analysis, a p-k solver then utilizes these GAFs to solve the aeroelastic stability problem [11].

2. Linearized Frequency Domain - Gust Perturbation Extension

For FVM-based gust linearization, the gust perturbations are assumed to be small harmonic perturbations of a gust profile, k, at frequency ω_k:

$$\mathbf{u}_G(t) := \sum_{k}^{n_k} \beta_n \hat{\mathbf{u}}_{G,k} e^{i\omega_k t}, \tag{10}$$

$$\mathbf{q}(t) := \mathbf{q}_0 + \sum_{k}^{n_k} \beta_k \hat{\mathbf{q}}_k e^{i\omega_k t}, \tag{11}$$

where $\hat{\mathbf{u}}_{G,k}$ is a spatially varying gust field corresponding to unit gust amplitude while β_k is the amplitude of the gust. These gust perturbations are about a steady equilibrium with zero gust amplitude. Linearizing and simplifying the governing equations with this form of the gust profile leads to:

$$\mathbf{A}_{gust,k}\left(\mathbf{x}_{G0}, \mathbf{q}_0, \hat{\mathbf{u}}_{G,k}, \hat{\mathbf{q}}_k\right) := \left(i\omega_k \left.\mathbf{M}_A\right|_{\mathbf{x}_{G0},\mathbf{q}_0} + \left.\frac{\partial \mathbf{R}}{\partial \mathbf{q}}\right|_{\mathbf{x}_{G0},\mathbf{q}_0}\right)\hat{\mathbf{q}}_\mathbf{k} + \left.\frac{\partial \mathbf{R}}{\partial \mathbf{u}_G}\right|_{\mathbf{x}_{G0},\mathbf{q}_0} \hat{\mathbf{u}}_{G,k} = 0. \tag{12}$$

As with Eq. 7, the linearizations are computed with automatic differentiation of the residual, and this equation is solved with SLAT in order to compute the linearized flow state. The spatial component of the gust profile, $\hat{\mathbf{u}}_{G,k}$, can take any arbitrary form. In this work, the harmonic gust perturbation field is defined as a vertical, sinusoidal gust convecting at the freestream velocity:

$$\hat{\mathbf{u}}_{G,k}\left(x\right) := \left[0, 0, e^{-j\omega_k x/M_\infty}\right]^T. \tag{13}$$

The vertical velocity component is only a spatial function of x. Once the linearized flow response to the gust perturbations is computed, the force perturbations can be computed:

$$\hat{\mathbf{f}}_n := \left.\frac{\partial \mathbf{f}}{\partial \mathbf{q}}\right|_{\mathbf{x}_{G0},\mathbf{q}_0} \hat{\mathbf{q}}_n + \left.\frac{\partial \mathbf{f}}{\partial \hat{\mathbf{u}}_G}\right|_{\mathbf{x}_{G0},\mathbf{q}_0} \hat{\mathbf{u}}_{G,n}, \tag{14}$$

and the inner product of these linearized forces with the mode shapes projected onto the aerodynamic surface leads to the gust-on-structure GAFs:

$$\bar{\mathbf{Q}}_{gs}\left(i\omega_k\right)_m := \mathbf{\Phi}_{A,m}^T \hat{\mathbf{f}}_k. \tag{15}$$

Unlike the modal perturbations version of LFD, only the frequency changes for the gust perturbation; therefore, at a given frequency, the gust-on-structure GAFs, $\bar{\mathbf{Q}}_{gs}\left(i\omega_k\right)$, are a vector representing the modal force for each mode due to the gust.

To verify the LFD gust solver, the linearized flow state is compared to a Fourier transform of a time-domain solution with small amplitude (an assumed linear approximation). The NACA 64A010 airfoil at Mach 0.4 is subjected to a vertical sinusoidal gust at a reduced frequency of 0.5. For the time-domain problem, the amplitude of the gust is $\hat{w} = 10^{-5}$, and the temporal discretization is a second-order backward-difference formulation with up to 10 pseudotime subiterations to converge the nonlinear problem at each time step. The time step size is chosen such that there are about 100 time steps per period of the gust. After 12 gust periods, the solution is approximately periodic, so a least-squares analysis over the next 3 gust periods applied to the perturbations from the steady state solution approximates the Fourier coefficients of the gust response. The Fourier coefficients computed by the least-squared analysis are then normalized by the gust amplitude to compare to an LFD solution. Figure 2 compares the real part of the LFD vertical velocity to the results of the time-domain problem; both plots show the sinusoidal wake generated by the oscillating gust impact on the airfoil. The contour plots appear essentially identical due to the limited precision from the contour color bands; however, Table 2 compares the LFD flow state to the time-domain equivalent at an arbitrarily chosen mesh node just above the leading edge of the airfoil. The two flow states agree to 3 to 5 significant digits, which is reasonably accurate when considering the gust amplitude in the time-domain problem.

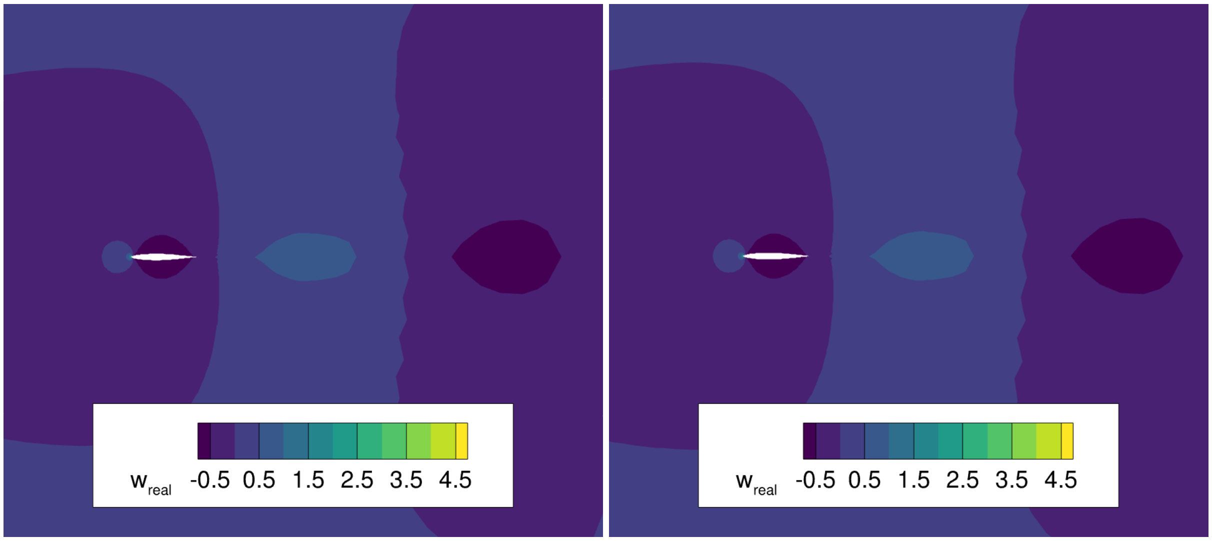

(a) Fourier transform of the time-domain solution. **(b) LFD.**

Fig. 2 Comparison of real part of the vertical velocity computed by LFD gust analysis and a Fourier transform of a time-domain analysis with a gust magnitude of 10^{-5}.

Table 2 Comparison of frequency-domain state vector at a node computed by LFD gust analysis and a Fourier Transform (FT) of a time-domain analysis with a gust magnitude of 10^{-5}.

Variable	Value
LFD $\hat{\rho}$	$-\mathbf{0.7548}15161228179932 + \mathbf{0.545}927464962005615j$
FT $\hat{\rho}$	$-\mathbf{0.7548}08783531188965 + \mathbf{0.545}866072177886963j$
LFD $\hat{u}$	$\mathbf{1.7779}7138690948486 - \mathbf{1.5403}9525985717773j$
FT $\hat{u}$	$\mathbf{1.7779}3002128601074 - \mathbf{1.5403}3589363098145j$
LFD $\hat{w}$	$-\mathbf{0.3968}69659423828125 - \mathbf{0.4044}74884271621704j$
FT $\hat{w}$	$-\mathbf{0.3968}85335445404053 - \mathbf{0.4044}46154832839966j$
LFD $\hat{T}$	$-\mathbf{0.3458}17238092422485 + \mathbf{0.25134}9925994873047j$
FT $\hat{T}$	$-\mathbf{0.3458}05108547210693 + \mathbf{0.25134}1730356216431j$

C. Stochastic Gust Analysis

To compute the stochastic gust response, the linearized structural dynamics equations for a given gust frequency, ω, are written in modally reduced form as:

$$\left[-\omega^2\bar{\mathbf{M}} + i\omega\bar{\mathbf{C}} + \bar{\mathbf{K}} - q_\infty \bar{\mathbf{Q}}_{ss}(i\omega)\right] \boldsymbol{\eta}(i\omega) = q_\infty \bar{\mathbf{Q}}_{gs}(i\omega), \tag{16}$$

where $\bar{\mathbf{M}}$, $\bar{\mathbf{C}}$, and $\bar{\mathbf{K}}$ are the generalized mass, damping, and stiffness matrices, respectively; q_∞ is the freestream dynamic pressure; and $\boldsymbol{\eta}(i\omega)$ is the frequency-domain generalized displacement vector. The structure-on-structure and gust-on-structure GAFs in Eq. 16 are interpolated for the small set of frequencies at which the LFD analyses are performed, typically around 10 to 15 frequencies. After solving Eq. 16 for the generalized displacement vector over a range of frequencies, the Power Spectral Density (PSD) of the gust response in some metric of interest can be computed as:

$$PSD(i\omega) := \left|\mathbf{S}^T \boldsymbol{\eta}(i\omega)\right|^2 f_{atm}(i\omega), \tag{17}$$

where $\mathbf{S}$ is a vector that transforms a unit generalized displacement to the quantity of interest, such as a tip displacement or root bending moment, and f_{atm} is a filter based on the frequency content of the atmosphere. In this work, the Dryden atmospheric turbulence model is used for f_{atm}. From the PSD, a Root Mean Square (RMS) can be computed:

$$RMS := \sqrt{\int_0^{\omega_{max}} PSD(i\omega) d\omega}. \tag{18}$$

The RMS of the quantity of interest is then the constraint applied to the optimization problem.

D. Implementation

The various components of the gust analysis process described above are integrated using OpenMDAO [27] and MPhys [28]. OpenMDAO is Python-based optimization framework that automates coupling of analyses and computation of coupled sensitivities. MPhys is a library that standardizes the integration of multiphysics problems for OpenMDAO.

The general analysis process is given in the extended design structure matrix (XDSM) diagram in Fig. 3. Given a set of shape design variables, the wing geometry component updates the structural mesh and aerodynamic surface mesh coordinates. The structural solver performs a modal decomposition of the structure. Next, the static aeroelastic problem is converged with a Nonlinear Block Gauss-Seidel (NLBGS) algorithm. Within the NLBGS loop, the displacement transfer projects the displacements from the structural mesh to the aerodynamic surface mesh, the aerodynamic solver updates its state and computes new forces on the aerodynamic surface, the load transfer projects these forces to the structural mesh, and the structural solver updates the displacements. After the static aeroelastic problem is complete, the mode shapes are transferred from the structural mesh to the aerodynamic surface, and then the gust subsystem performs the linearized gust analysis outlined in the following paragraph. The load and displacement transfers as well as the mode shape transfer are performed with the Matching-based Extrapolation of Load and Displacements (MELD) approach [29]. The structural analysis is performed with an in-house finite element solver.

The parts of the linearized gust analysis subsystem from Fig. 3 are given in Fig. 4. The mode shapes projected onto the aerodynamic surface are used to compute displacements of the CFD volume mesh due to a unit mode shape perturbation. These volume mesh displacements feed the LFD motion perturbation component, which solves for the linearized flow responses due to perturbations of each mode over a range of prescribed frequencies (Eq. 7). From the linearized flow states, the structure-on-structure GAFs are computed using Eqs. 8 and 9. Next, the LFD response due to gust perturbations are computed with Eq. 12 for the same range of prescribed frequencies as the motion perturbation LFD analysis. The gust-on-structure GAFS are then computed with Eqs. 14 and 15. After both sets of linearized flow analyses, the quantity of interest identifier component (QOI ID) generates the $\mathbf{S}$ vector necessary for Eq. 17. Finally, the gust RMS component solves the stochastic gust response problem in Eqs. 16–18 to compute the RMS of the quantity of interest.

Since OpenMDAO creates copies of all the declared states, the implementation combines the LFD solvers and corresponding GAF computations into a single subsystem for each perturbation type to reduce the memory requirements, i.e., the $\hat{\mathbf{q}}$ vectors are hidden from OpenMDAO to prevent it from making large allocations of memory to store all the linearized states simultaneously. Inside these combined LFD-GAF components, file input/output shuffles the linearized states into and out of memory as needed.

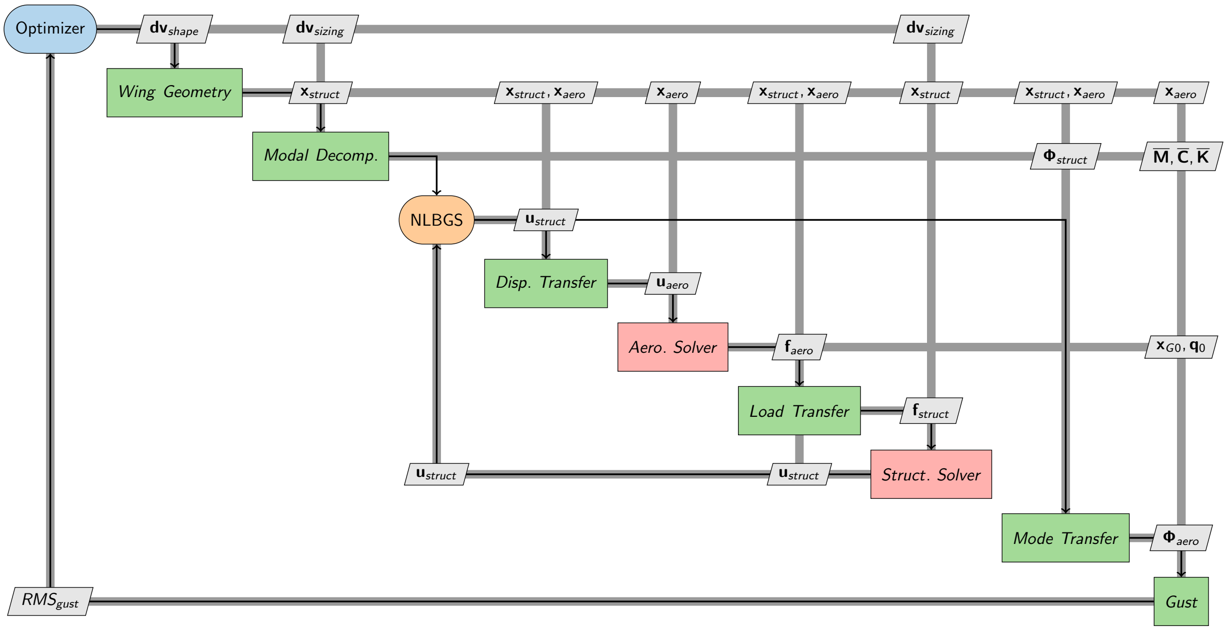

Fig. 3 General XDSM diagram of the gust constraint assembled in OpenMDAO by MPhys.

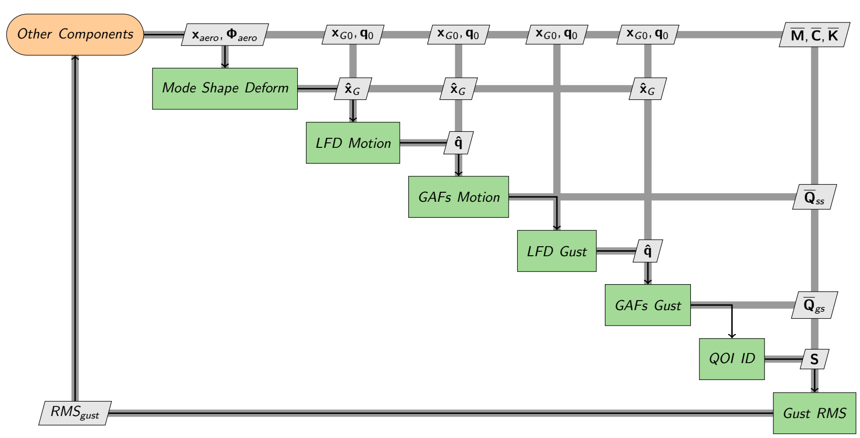

Fig. 4 XDSM diagram of the gust analysis subsystem based on LFD.

III. Adjoint-based Sensitivities

One of the key benefits of OpenMDAO is the automation of the coupled sensitivities for all of the steps in Figs. 3 and 4; however, this still requires that each component provide linearizations of its outputs or residuals with respect to its inputs. For the large analysis components such as the flow analysis steps, these are implemented as matrix-free Jacobian vector products.

Some of the same challenges for the LFD-based flutter sensitivities in Jacobson et al. [12] are common to the gust sensitivity analysis, namely the lack of complex-differentiability of the cost function and the need for second derivatives of the RANS equations for the LFD-based aerodynamics. The RMS cost function has complex-valued inputs (the GAFs) but produces a real-valued output; this means that the Cauchy-Riemann equations for complex differentiability are not satisfied. The adjoint equations modified to account for the lack of complex differentiability were derived in the previous work (see Equation 24 of Ref. [12]). The modified equations essentially require that the linearization of the cost function with respect to any complex state requires the sign of the imaginary part be flipped; this is implemented in the gust RMS OpenMDAO component for the derivatives of the output RMS with respect to the structure-on-structure and gust-on-structure GAFs.

As with the structural mode perturbation form of LFD, Eq. 12 is a linearization of the Navier-Stokes equations; therefore, computing the linearizations of the residual with respect to the inputs requires second derivatives of the governing equations of the flow. For example, the linearization of the gust LFD equation with respect to the mean flow state is required:

$$
\begin{aligned}
\left[\frac{\partial \mathbf{A}_{gust}}{\partial \mathbf{q}_0}\right]^T \psi_{A_{gust},k} = & \left[\frac{\partial}{\partial \mathbf{q}}\left(i\omega_k\, \mathbf{M}_A|_{\mathbf{x}_{G0},\mathbf{q}_0}\hat{\mathbf{q}}_k\right)\right]^T \psi_{A_{gust},k} \\
& + \left[\frac{\partial}{\partial \mathbf{q}}\left(\left.\frac{\partial \mathbf{R}}{\partial \mathbf{q}}\right|_{\mathbf{x}_{G0},\mathbf{q}_0}\hat{\mathbf{q}}_k\right)\right]^T \psi_{A_{gust},k} \\
& + \left[\frac{\partial}{\partial \mathbf{q}}\left(\left.\frac{\partial \mathbf{R}}{\partial \mathbf{u}_G}\right|_{\mathbf{x}_{G0},\mathbf{q}_0}\hat{\mathbf{u}}_{G,k}\right)\right]^T \psi_{A_{gust},k}.
\end{aligned}
\tag{19}
$$

Because these terms need matrix vector products with these second derivatives, complex-step directional derivatives of analytical first derivatives can be used. Complex-step derivatives are finite difference estimations that perturb the imaginary part of the real-valued functions [30–32]. Unlike real-valued finite differencing, complex-step derivatives do not suffer from subtractive cancellation error, and extremely small steps produce accurate derivatives. Complex-step sizes of 10^{-30} are utilized in this work. Using complex-step directional derivatives and some manipulation of the expression, the third term from Eq. 19 is computed as:

$$
\begin{aligned}
\Re\left(\frac{\partial}{\partial \mathbf{u}_G}\left(\left.\frac{\partial \mathbf{R}}{\partial \mathbf{q}}\right|^T_{\mathbf{x}_{G0},\mathbf{q}_0,\mathbf{u}_G=0}\psi_{A_{gust},k}\right)\hat{\mathbf{u}}_{G,k}\right) = & \frac{\Im\left(\left.\frac{\partial \mathbf{R}}{\partial \mathbf{q}}\right|^T_{\mathbf{x}_{G0},\mathbf{q}=\mathbf{q}_0,\mathbf{u}_G=ih\,\Re(\hat{\mathbf{u}}_{G,k})}\Re\left(\psi_{A_{gust},k}\right)\right)}{h} \\
& - \frac{\Im\left(\left.\frac{\partial \mathbf{R}}{\partial \mathbf{q}}\right|^T_{\mathbf{x}_{G0},\mathbf{q}=\mathbf{q}_0,\mathbf{u}_G=ih\,\Im(\hat{\mathbf{u}}_{G,k})}\Im\left(\psi_{A_{gust},k}\right)\right)}{h}.
\end{aligned}
\tag{20}
$$

In these expressions, $\Re$ and Im represent the real and imaginary parts of the arguments, respectively. The analytical derivatives in FUN3D/SFE are computed with operator-overloaded automatic differentiation. The mean flow state is real-valued, so only the real part of the matrix-vector product is required. Because the gust profile and adjoint states are complex-valued, computing the real part of the term requires two complex-step directional derivatives, where the first one is the term from the real part of both states, and the second term is the result of the product of the imaginary parts. This process for linearization is applied for all of the linearizations of Eqs. 7, 8, 12, and 14 with respect to the mean flow state and grid coordinates.

Dot-product tests have been performed to check the accuracy of all the required linearization terms. For the dot-product test, random perturbation vectors for the input $\mathbf{v}'$ and residual $\mathbf{R}'$ are generated. Then the following products should hold for any of the residuals and inputs:

$$
\mathbf{R}'^T\left(\frac{\partial \mathbf{R}}{\partial \mathbf{v}}\mathbf{v}'\right) = \mathbf{v}'^T\left(\frac{\partial \mathbf{R}}{\partial \mathbf{v}}^T\mathbf{R}'\right),
\tag{21}
$$

Table 3 Dot-product test for linearizations of the LFD gust residual with respect to the mean flow state.

Method	Value
Analytical - Forward	**1152121.88304295**
Analytical - Reverse	**1152121.88304295**
Finite Difference ($h = 10^{-8}$)	**1**669547.47515755
Finite Difference ($h = 10^{-9}$)	**11**47297.44609761
Finite Difference ($h = 10^{-10}$)	**115212**3.47213434
Finite Difference ($h = 10^{-11}$)	**11521**50.86663199
Finite Difference ($h = 10^{-12}$)	**11521**41.70419460
Finite Difference ($h = 10^{-13}$)	**115**3795.01893256

Table 4 Verification of the derivative of the stochastic gust constraint function with respect to design variables for the AGARD 445.6 wing.

Method	Structural Thickness	Sweep
Analytical - Reverse	**−3.487636565298064**	**−0.028985445010219**
Finite Difference ($h = 10^{-2}$)	**−3.4**41091464667863	**−0.0289**51549078215
Finite Difference ($h = 10^{-3}$)	**−3.48**3042198356543	**−0.02898**206800478
Finite Difference ($h = 10^{-4}$)	**−3.487**177661110763	**−0.028985**128032218
Finite Difference ($h = 10^{-5}$)	**−3.487**590761040337	**−0.028985**785116674
Finite Difference ($h = 10^{-6}$)	**−3.48763**1555646658	**−0.02898**800582625
Finite Difference ($h = 10^{-7}$)	**−3.4876**25617533922	**−0.02898**9844024181
Finite Difference ($h = 10^{-8}$)	**−3.487**759321928024	**−0.02**9095768928528

where the left hand side is a forward mode linearization either analytically computed or with finite differencing, and the right hand side is the reverse mode (adjoint) version computed analytically. Table 3 shows the dot-product test for the linearization of Eq. 12 with respect to the mean flow state, $\mathbf{q}_0$. The analytical solutions based on complex-step directional derivatives like Eq. 20 match to double precision. The finite-difference results have fairly significant sensitivity to the step size, but the step size of 10^{-10} match the analytical versions to six digits. Since the primal analysis contains complex numbers, the verification of this term must be done with real-valued finite differencing.

With the individual linearization terms implemented in OpenMDAO components and verified using dot-product tests, OpenMDAO automates the coupling of the full sensitivities to allow computation of the sensitivities of a gust RMS cost function with respect to design variables. Table 4 shows the verification of derivatives of the stochastic gust cost function, RMS of the wing tip displacement, with respect to two design variables from the optimization problem in the next section: panel thickness of the structural model and sweep where the geometric changes that affect both the structural and aerodynamic models. Both derivatives have good agreement with the real-valued finite differencing with about 5–6 significant digits of agreement using step sizes of 10^{-5} to 10^{-6}.

IV. Optimization

The optimization problem applies the stochastic gust constraint to the AGARD 445.6 wing [14]. The AGARD 445.6 wing has an aspect ratio of 1.65, a sweep angle of 45°, and a taper ratio of 0.66. Since the airfoil is symmetric, there is no twist, and the simulated angle of attack is 0°, the static aeroelastic coupling loop in Fig. 3 is replaced by a single aerodynamic evaluation in this problem. The structural model consists of the 100 shell elements shown in Fig. 5. The freestream Mach number is 0.5, and the motion and gust LFD analyses are performed for 11 reduced frequencies between $k = 0$ and $k = 2.0$. Two versions of the optimization problem are performed; the first one is based on the LFD process described above, and the second one replaces LFD with linear aerodynamics based on the Doublet-Lattice

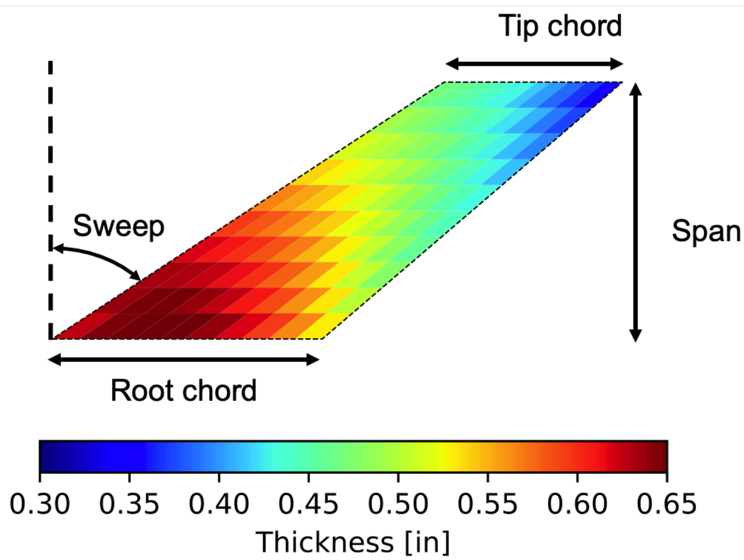

Fig. 5 Design parameterization and initial AGARD 445.6 wing configuration. The flow direction is left to right.

Method (DLM). The LFD-based optimization uses inviscid aerodynamics with a mesh containing 219,555 nodes. Since the flow conditions are within the linear regime, the expectation is that the two versions of the optimization should produce similar results.

The optimization problem minimizes the mass of the AGARD 445.6 wing subject to a constraint on the RMS of the vertical displacement of the wingtip trailing edge when subjected to a stochastic gust load while a second constraint ensures that the planform area does not change:

$$\begin{aligned} \text{min} \quad & mass \\ \text{subject to:} \quad & RMS_{z,tip} \leq 1.5 \\ & A = A_0. \end{aligned} \tag{22}$$

The tip displacement RMS is limited to 1.5 inches. There are 104 total design variables in Fig. 5: the thickness of the 100 structural elements and the 4 planform variables that control the span, sweep, and root and tip chord. The geometric variables affect both the structural model and the aerodynamic outer mold line. For the initial design, the LFD-based RMS of the tip displacement is 1.88 in, and the DLM-based RMS is 1.94 in; both of these violate the constraint limit. The optimizations are performed with the sequential least-squares quadratic programming (SLSQP) optimizer [33] with the convergence tolerance set to 10^{-4}. The LFD and DLM optimizations converge to the tolerance in 33 and 46 iterations, respectively. The convergence histories are given in Fig. 6. The LFD optimization reduces the mass of the wing by 26.4% compared to 24.1% for the DLM. This difference is likely related to the differences in the initial RMS of the tip displacement where the LFD predicts 3.1% less tip displacement on the same design. Figure 7 compares the final DLM and LFD designs. As expected, the designs are very similar with both versions reducing the wingspan to the allowed minimum and strengthening the trailing edge near the root. For the LFD design, the panel thicknesses near the root trailing edge are slightly thinner, which is consistent with the total mass being less.

The LFD optimization is run on 400 Intel Skylake CPU cores. Average wall time for function and gradient calls are 70.5 and 146.4 minutes, respectively. The DLM optimization is run on 40 Skylake CPU cores. Average DLM wall times are 0.5 and 7.7 seconds, respectively, for the function and gradient calls, totaling a little over 6 minutes for a full optimization. While focusing on correctness for this work, essentially no effort has been made to improve the performance of the LFD analysis. There are many areas of the LFD process that can be sped up, but the computational cost of the DLM will always be significantly lower than the LFD. The modularity of OpenMDAO and MPhys permits easy swapping of fidelities, so optimizations can be performed with both aerodynamics models in the same problem. In future work, the higher fidelity gust analysis only needs to be applied when DLM is insufficient, e.g., transonic conditions. Or when the higher accuracy of the LFD is desired, an LFD-based optimization can be initialized from the optimal DLM-based design.

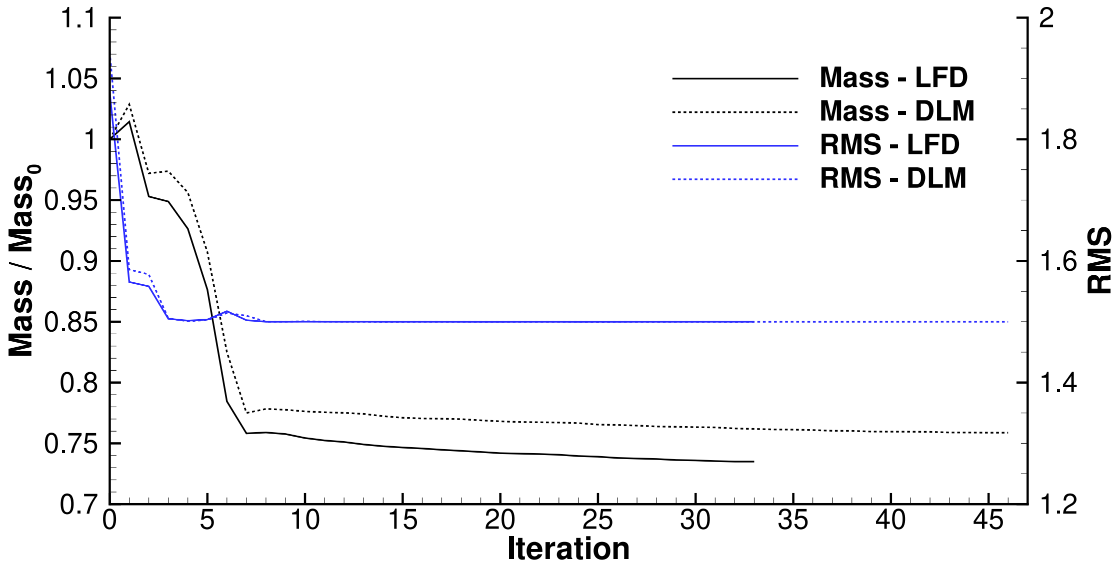

Fig. 6 Optimization history for the gust-constraint mass minimization of the AGARD 445.6.

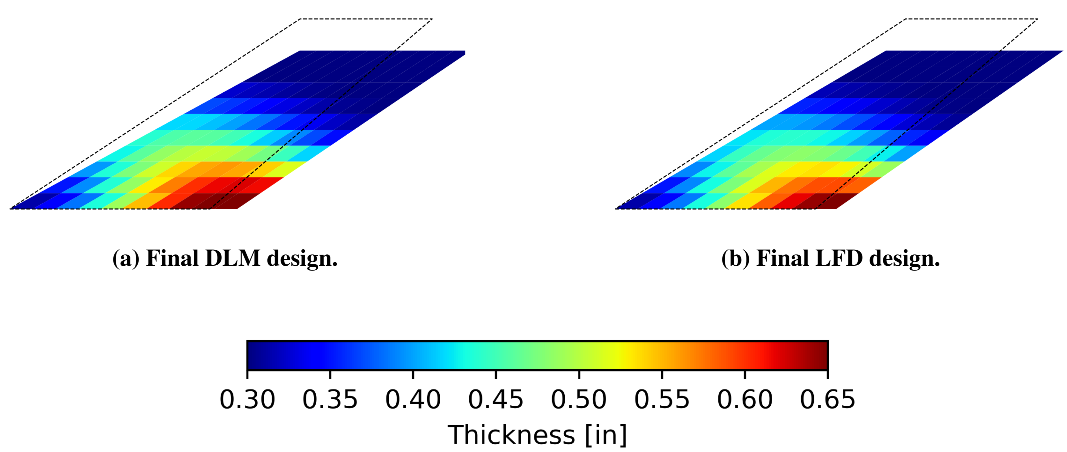

Fig. 7 AGARD 445.6 planform and thickness distributions. The flow direction is left to right.

V. Conclusions

In this work, an LFD gust analysis has been added to FUN3D/SFE. Using OpenMDAO and MPhys, the LFD aerodynamics are combined with structural dynamics and atmospheric turbulence models to perform stochastic gust analysis. The stochastic gust analysis and adjoint-based sensitivities have been verified, and an initial optimization has been performed minimizing the mass of the AGARD 445.6 wing subject to a stochastic gust constraint on the wingtip displacement. The LFD-based optimization converged to results that agree with DLM-based gust analysis at a flight condition where both aerodynamic models are applicable. The presented optimization proves that the LFD-based process and sensitivities can be applied in an optimization problem with stochastic gust constraints. In future work, this capability will be applied to transonic conditions, where the DLM is not applicable, and to more complex configurations, such as the NASA Common Research Model optimization problems in Thelen et al. [34].

Acknowledgments

This work is supported by the Transformational Tools and Technologies (TTT) project of the NASA Transformative Aeronautics Concepts Program (TACP). Computational resources for this work were provided by the NASA Langley K cluster.

References

[1] Bartels, R. E., Stanford, B., and Waite, J., "Performance Enhancement of the Flexible Transonic Truss-Braced Wing Aircraft Using Variable-Camber Continuous Trailing-Edge Flaps," *AIAA Aviation Forum*, Dallas, Texas, 2019.

[2] Wang, Z., Yang, S., and Chen, P.-C., "Aeroelastic Analysis Using FUN3D-Based ROM Simultaneously Subject to Gust and Control Surface Deflections," *AIAA Scitech Forum*, San Diego, California, 2019.

[3] Stanford, B., "Aeroservoelastic Optimization under Stochastic Gust Constraints," *AIAA Aviation Forum*, American Institute of Aeronautics and Astronautics, 2018.

[4] Stanford, B., "Optimal Aircraft Control Surface Layouts for Maneuver and Gust Load Alleviation," *AIAA Scitech Forum*, Orlando, Florida, 2020.

[5] Jacobson, K. E., "Adjoint-based Aeroelastic Optimization with High-fidelity Time-accurate Analysis," Ph.D. thesis, Georgia Institute of Technology, Atlanta, Georgia, 2018.

[6] Hall, K. C., Thomas, J. P., and Clark, W. S., "Computation of Unsteady Nonlinear Flows in Cascades Using a Harmonic Balance Technique," *AIAA Journal*, Vol. 40, No. 5, 2002, pp. 879–886.

[7] Thomas, J. P., Dowell, E. H., and Hall, K. C., "Modeling Viscous Transonic Limit Cycle Oscillation Behavior Using a Harmonic Balance Approach," *Journal of Aircraft*, Vol. 41, No. 6, 2004, pp. 1266–1274.

[8] He, S., Jonsson, E., Mader, C. A., and Martins, J. R. R. A., "A Coupled Newton-Krylov Time Spectral Solver for Wing Flutter and LCO Prediction," *AIAA Aviation Forum*, Dallas, Texas, 2019.

[9] Widhalm, M., Dwight, R. P., Thormann, R., and Hübner, A., "Efficient Computation of Dynamic Stability Data with a Linearized Frequency Domain Solver," *Proceedings of the European Conference on Computational Fluid Dynamics*, Lisbon, Portugal, 2010.

[10] Widhalm, M., and Thormann, R., "Efficient Evaluation of Dynamic Response Data with a Linearized Frequency Domain Solver at Transonic Separated Flow Condition," *35th AIAA Applied Aerodynamics Conference*, 2017.

[11] Jacobson, K. E., Stanford, B. K., Wood, S. L., and Anderson, W. K., "Flutter Analysis with Stabilized Finite Elements based on the Linearized Frequency-domain Approach," *58th AIAA Aerospace Sciences Meeting*, Orlando, Florida, 2020.

[12] Jacobson, K. E., Stanford, B. K., Wood, S. L., and Anderson, W. K., "Adjoint-based Sensitivities of Flutter Predictions based on the Linearized Frequency-domain Approach," *59th AIAA Aerospace Sciences Meeting*, Virtual Event, 2021.

[13] Jacobson, K. E., and Stanford, B. K., "Flutter-Constrained Optimization with the Linearized Frequency-Domain Approach," *AIAA SciTech Forum*, San Diego, California, 2022.

[14] Yates, C. E., "AGARD Standard Aeroelastic Configurations for Dynamic Response. Candidate Configuration I - Wing 445.6," Tech. Rep. TM-100492, NASA, August 1 1987.

[15] Anderson, W. K., and Bonhaus, D. L., "An Implicit Upwind Algorithm for Computing Turbulent Flows on Unstructured Grids," *Computers & Fluids*, Vol. 23, No. 1, 1994, pp. 1–21.

[16] Biedron, R. T., and Thomas, J. L., "Recent Enhancements to the FUN3D Flow Solver for Moving-Mesh Applications," *AIAA 47th Aerospace Sciences Meeting*, Orlando, Florida, 2009.

[17] Nielsen, E. J., and Anderson, W. K., "Recent Improvements in Aerodynamic Design Optimization on Unstructured Meshes," *AIAA Journal*, Vol. 40, 2002, pp. 1155–1163.

[18] Wang, L., Diskin, B., Biedron, R., Nielsen, E. J., and Bauchau, O., "Sensitivity Analysis of Multidisciplinary Rotorcraft Simulations," *55th AIAA Aerospace Sciences Meeting*, 2017, p. 1670.

[19] Anderson, W. K., Newman, J. C., and Karman, S. L., "Stabilized Finite Elements in FUN3D," *55th AIAA Aerospace Sciences Meeting*, 2017.

[20] Anderson, W. K., and Newman, J., "High-Order Stabilized Finite Elements on Dynamic Meshes," *2018 AIAA Aerospace Sciences Meeting*, 2018.

[21] Allmaras, S. R., Johnson, F. T., and Spalart, P. R., "Modifications and Clarifications for the Implementation of the Spalart-Allmaras Turbulence Model," 2012.

[22] Singh, R., and Baeder, J. D., "Direct Calculation of Three-Dimensional Indicial Lift Response Using Computational Fluid Dynamics," *Journal of Aircraft*, Vol. 34, No. 4, 1997, pp. 465–471. doi:10.2514/2.2214.

[23] Boulbrachene, K., De Nayer, G., and Breuer, M., "Assessment of Two Wind Gust Injection Methods: Field Velocity Versus Split Velocity Method," *Journal of Wind Engineering and Industrial Aerodynamics*, Vol. 218, 2021, p. 104790.

[24] Bartels, R. E., "Development, Verification and Use of Gust Modeling in the NASA Computational Fluid Dynamics Code FUN3D," Tech. rep., 2012.

[25] Saad, Y., and Schultz, M., "GMRES: a Generalized Minimal Residual Algorithm for Solving Nonsymmetric Linear Systems," *Siam Journal on Scientific and Statistical Computing*, Vol. 7, 1986, pp. 856–869.

[26] Wood, S. L., Jacobson, K. E., Jones, W. T., and Anderson, W. K., "Sparse Linear Algebra Toolkit for Computational Aerodynamics," *58th AIAA Aerospace Sciences Meeting*, Orlando, Florida, 2020.

[27] Gray, J. S., Hwang, J. T., Martins, J. R. R. A., Moore, K. T., and Naylor, B. A., "OpenMDAO: An Open-Source Framework for Multidisciplinary Design, Analysis, and Optimization," *Structural and Multidisciplinary Optimization*, Vol. 59, 2019, pp. 1075–1104.

[28] Yildirim, A., Jacobson, K. E., Stanford, B. K., Gray, J. S., Mader, C. A., Martins, J. R. R. A., and Kennedy, G. J., "MPhys: A Modular Multiphysics Simulation Package using the OpenMDAO Framework," *AIAA Aviation Forum*, Presentation Only, Virtual, 2020.

[29] Kiviaho, J. F., and Kennedy, G. J., "Efficient and Robust Load and Displacement Transfer Scheme Using Weighted Least Squares," *AIAA Journal*, Vol. 57, No. 5, 2019, pp. 2237–2243.

[30] Lyness, J., "Numerical Algorithms based on the Theory of Complex Variable," *Proceedings of the 1967 22nd national conference*, ACM, 1967, pp. 125–133.

[31] Anderson, W. K., Newman, J. C., Whitfield, D. L., and Nielsen, E. J., "Sensitivity Analysis for Navier-Stokes Equations on Unstructured Meshes Using Complex Variables," *AIAA Journal*, Vol. 39, No. 1, 2001, pp. 56–63. doi:10.2514/2.1270, URL `https://doi.org/10.2514/2.1270`.

[32] Martins, J., Sturdza, P., and Alonso, J., "The Complex-step Derivative Approximation," *ACM Transactions on Mathematical Software (TOMS)*, Vol. 29, No. 3, 2003, pp. 245–262.

[33] Kraft, D., "A Software package for Sequential Quadratic Programming," Tech. Rep. DFVLR-FB 88-28, Köln, Germany, 1988.

[34] Thelen, A. S., Stanford, B. K., and Jacobson, K. E., "Flutter and Stochastic Gust Constraint Studies of the Undeflected CRM using MPhys," *AIAA Scitech 2024 Forum*, 2024, submitted.